Topology of high-dimensional chaotic scattering

Ying-Cheng Lai,[1] Alessandro P. S. de Moura,[2] and Celso Grebogi[2,3]
[1]*Department of Mathematics, Department of Electrical Engineering, and Department of Physics, Center for Systems Science and Engineering Research, Arizona State University, Tempe, Arizona 85287-1804*
[2]*Institute for Plasma Research, University of Maryland, College Park, Maryland 20742*
[3]*Department of Mathematics, Institute for Physical Science and Technology, University of Maryland, College Park, Maryland 20742*
(Received 7 July 2000)

We investigate Hamiltonian chaotic scattering in physically realistic three-dimensional potentials. We find that the basin topology of the scattering dynamics can undergo a metamorphosis from being totally disconnected to being connected as a system parameter, such as the particle energy, is varied through a critical value. The dynamical origin of the metamorphosis is investigated, and the topological change in the scattering basin is explained in terms of the change in the structure of the invariant set of nonescaping orbits. A dynamical consequence of this metamorphosis is that the fractal dimension of the chaotic set responsible for the chaotic scattering changes its behavior characteristically at the metamorphosis. This topological metamorphosis has no correspondence in two-degree-of-freedom open Hamiltonian systems.

PACS number(s): 05.45.Jn

I. INTRODUCTION

Chaotic scattering is a phenomenon that has been identified in many physical contexts such as atomic physics [1], astrophysics [2], fluid dynamics [3], chemical reactions [4], and electron transport in mesoscopic systems [5]. In a chaotic scattering process, the plot of some output variable, such as the scattering function, after the scattering versus some input variable before the scattering typically contains an uncountably infinite number of singularities. The output of the system then depends sensitively on the input in that a small change in the input variable can cause a large change in the output—this being the hallmark of chaos. Dynamically, chaotic scattering is caused by nonattracting chaotic saddles in the phase space and it is a direct manifestation of transient chaos in physical systems [6,7].

A fundamental problem in the study of chaotic scattering is to understand how the scattering characteristics change as a system parameter of physical interest changes. In this regard, there has been research on two-degree-of-freedom Hamiltonian systems [8–10] and on three-degree-of-freedom Hamiltonian systems but with hard-wall potentials [11]. The aim of this paper is to investigate chaotic scattering in three-degree-of-freedom Hamiltonian systems consisting of physically realistic soft potentials. Our motivation comes from the desire to understand the dynamics in phenomena such as the scattering of particles by molecules in three-dimensional physical space. In phase space, the scattering dynamics is then five dimensional. We use a particular model of four Morse potential hills in a tetrahedron configuration, but this model is sufficiently general to allow us to draw conclusions on high-dimensional systems, besides being interesting and physically realistic by itself. Our principal results are (1) the topology of the chaotic scattering dynamics can undergo a sudden change (a *metamorphosis*), as a system parameter (e.g., energy) changes continuously, (2) at the topological metamorphosis, the behavior of the fractal dimension of the chaotic saddle changes characteristically, and (3) chaotic scattering can occur in energy regimes where it is not possible in the corresponding planar scattering system. We note that the related transient chaotic dynamics in such high-dimensional phase space is a defying problem that has not been well studied so far.

The paper is organized as follows. In Sec. II the scattering model is described. In Sec. III we present evidence for chaotic scattering by studying the scattering functions. In Sec. IV the topological metamorphosis of the scattering dynamics is addressed. In Sec. V the change in the invariant set at the metamorphosis is studied on an invariant plane of the potential. A conclusion is presented in Sec. VI.

II. MODEL

We consider the following class of three-degree-of-freedom, time-independent Hamiltonian systems: $H(\mathbf{x},\mathbf{p}) = |\mathbf{p}|^2/2m + V(\mathbf{x})$, where $\mathbf{x},\mathbf{p} \in \mathbb{R}^3$ are the coordinate and momentum vectors, and m is the particle mass. To be more specific and without loss of generality, we study the situation where there are four potential hills, located at the four vertices of a regular tetrahedron of unit side lengths, in the three-dimensional physical space. The locations of the vertices of the tetrahedron are $(x_1,y_1,z_1)=(0,0,\sqrt{2/3})$, $(x_2,y_2,z_2) = (1/2,-1/(2\sqrt{3}),0)$, $(x_3,y_3,z_3)=(-1/2,-1/(2\sqrt{3}),0)$, and $(x_4,y_4,z_4)=(0,\sqrt{1/3},0)$, as shown in Fig. 1. To mimic physical situations such as particle scattering by nonrotating diatomic molecules, we choose the Morse potential [12] for each hill, which has been a paradigm in chemical and atomic physics [13]. The potential due to each Morse hill is $V_M(\mathbf{x})$, where $\mathbf{x}=(x,y,z)$, and

$$V_M(\mathbf{x}) = \frac{V_0}{2}[1-e^{-\alpha(r_j-r_e)}]^2 - \frac{V_0}{2}, \tag{1}$$

where $r_j = \sqrt{(x-x_j)^2+(y-y_j)^2+(z-z_j)^2}$, and V_0, α, and r_e are parameters of the Morse potential. α is related to the steepness of the potential, and r_e is the effective range of

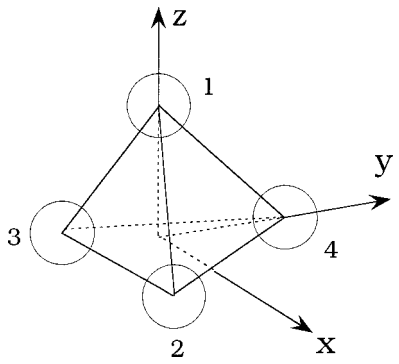

FIG. 1. A schematic illustration of the scattering system: four Morse potential hills located at the vertices of a regular tetrahedron.

each potential hill. The additive constant $-1/2$ ensures that $V_M(\mathbf{x})\to 0$ for $r\to\infty$. Each Morse hill is spherically symmetric and has a repulsive region, around $\mathbf{x}=\mathbf{x}_j$, surrounded by an attractive region. For $r\gg r_e$, the potential is negligible, and the particles there can be considered to be in free motion. We notice that although we chose to work with the Morse potential, our results are expected to be qualitatively the same for any short-range potential with a repulsive core and an attractive tail, such as the Lennard-Jones potential.

The dimensionless potential function of our scattering system can then be written as

$$V(x,y,z)=\sum_{j=1}^{4} V_M(\mathbf{x}). \tag{2}$$

Due to the conservation of energy, the phase-space dimension is five. In our work, we fix the following set of parameter values $m=1$, $V_0=1$, $\alpha=6$, $r_e=0.68$, and we choose the particle energy E as the bifurcation parameter. Equivalently, we could have chosen some other parameter, say V_0. Hamilton's equations are integrated by using the Störmer-Verlet method which preserves the symplectic structure of the system [14]. We note that the potential distribution is highly localized and we denote the region around $(x,y,z)=(0,0,0)$, in which $V(x,y,z)$ is appreciable, the scattering region.

We now focus our attention on the region of the three-dimensional physical space that is inaccessible to a particle with energy E. This region is given by $V(\mathbf{x})>E$. Throughout this paper, we restrict ourselves to energies below the maximum energy of the potential hills: $E<E_0=V(x_j,y_j,z_j)$ $(j=1,...,4)$ [15]. For energies higher than a certain critical energy E_c (and lower than E_0), the inaccessible part of space consists of four disconnected regions, each surrounding one vertex of the tetrahedron, as shown in Fig. 2(a); they are approximately spherical in shape (they are not perfectly spherical because their shape is distorted by the other hills). As the energy decreases towards E_c, the inaccessible regions grow in radius, and at $E=E_c$ the previously disconnected regions touch each other. By symmetry, every pair of two previously disconnected regions must touch each other at $E=E_c$. For $E\leqslant E_c$, the forbidden region is fully connected; an example is shown in Fig. 2(b). This topological change in the configuration space causes a corresponding change in the dynamics of the system, as can be understood by analyzing

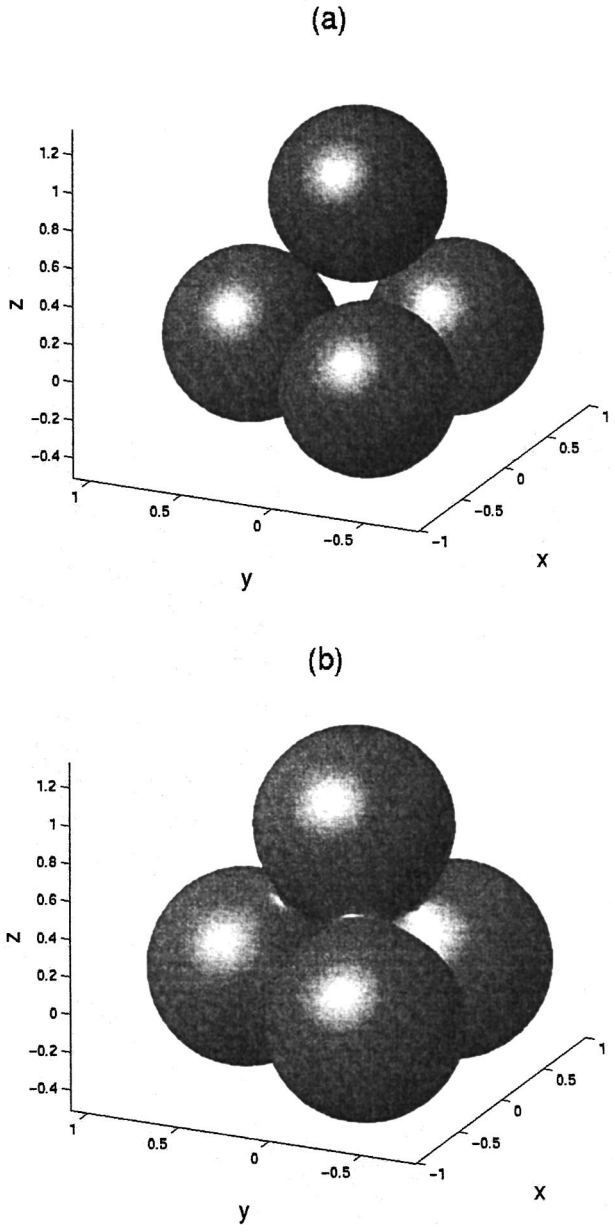

FIG. 2. Surfaces of equal energy for the potential (2) for energies above and below the critical energy E_c. (a) Isoenergy surface for $E=1$ $(E<E_c)$; (b) isoenergy surface for $E=4(E>E_c)$.

the invariant set, which is the set of orbits that do not leave the scattering region for both $t\to+\infty$ and $t\to-\infty$. As the energy drops below E_c, a whole family of orbits in the invariant set is destroyed, consisting of orbits that bounce back and forth between each pair of forbidden regions an arbitrary number of times, including the six unstable periodic orbits connecting each pair of hills that exist for $E>E_c$. As these orbits are destroyed, however, another family of orbits is created at $E=E_c$; these orbits bounce off the newly created forbidden regions connecting each pair of hills. We will describe this change in the invariant set in more detail later. This qualitative (that is, topological) change in the dynamics of the system at E_c is the metamorphosis that is the main subject of this paper.

The critical energy E_c can be estimated as follows. Consider the three Morse potentials in the (x, y) plane in Fig. 1.

For each individual potential, the radius of the classically forbidden spherical region is $r=r_e-(1/\alpha)\ln(1+\sqrt{2E/V_0})$. If there is no overlapping between the potentials, two adjacent potentials touch each other at $r=1/2$. Thus, E_c is approximately determined by

$$r_e-\frac{1}{\alpha}\ln\left(1+\sqrt{\frac{2E_c}{V_0}}\right)\approx 1/2.$$

We obtain $E_c\approx 1.9$. Due to the overlapping among potentials, the actual value of E_c will be slightly higher than this estimated one. In fact, we find numerically $E_c\approx 2.25$.

The basic physics associated with the topological metamorphosis can be understood in terms of the structural change in the ''holes'' on each side plane of the tetrahedron potential configuration as the particle energy is decreased. For $E>E_c$, the forbidden regions surrounding the vertices of the tetrahedron are isolated. For $E<E_c$ they are connected, and an incoming particle can penetrate the interior of the tetrahedron through the holes on the side planes. For the set of parameters chosen by us, the holes in the central regions of the side planes are always present, because of the attractive parts of each Morse hill. This allows particles to enter the scattering region inside the tetrahedron at low energies. For $E\lesssim E_c$, the holes are large and, hence, the range of initial conditions with which particles can enter the holes are appreciable. In this case, chaotic scattering can be readily observed. The holes, however, become smaller as E is decreased further from E_c. In particular, if there is no overlapping between the potentials, the size of the holes is given by

$$s\approx\frac{\sqrt{3}-1}{2}+\frac{1}{\alpha}\ln\frac{1+\sqrt{2E/V_0}}{1+\sqrt{2E_c/V_0}}.$$

For E slightly below E_c so that $(E_c-E)/E_c\equiv\Delta E/E_c\ll 1$, we have

$$s\approx C-h(E_c)\Delta E, \tag{3}$$

where $C=(\sqrt{3}-1)/2$ and $h(E_c)=1/[\alpha\sqrt{2E_c/V_0}(1+\sqrt{2E_c/V_0})]$. Thus, to observe chaotic scattering at very low energies in an experimental setting, initial conditions have to be prepared carefully so that particles can enter the holes, as the scattering will not be chaotic if the particles stay outside the holes (no unstable periodic orbit can be formed there for $E<E_c$, as can be seen in Fig. 3).

III. SCATTERING FUNCTIONS

We now analyze the scattering of test particles by the potential V of Eq. (2) by means of a scattering function defined as follows. Particles are launched towards the scattering region with a fixed velocity from a line segment, say aligned along the x direction, located far away from the scattering region, where $V\approx 0$. Each particle will enter the scattering region, stay there for a certain time, and typically leave towards $r\to\infty$ again. The scattering function characterizes the dynamical state, such as the direction of the particle motion, after leaving the scattering region. Since the physical space is three dimensional, there are two angles characterizing the momentum of a scattering particle: the azimuthal angle ϕ and the polar angle θ. Figure 4(a) shows, for $E=4$, the plot of ϕ after the scattering versus x_0, where particles are launched upwards with $p_{x0}=p_{y0}=0$, $p_{z0}=\sqrt{2E}$ at $z_0=-10.0$, and the scattering function $\phi(x_0)$ is recorded when the particles exit the scattering region, say, when $r\geqslant 10$. The plot exhibits typical features of chaotic scattering [8]: regions of smooth variations interspersed by abrupt changes in the scattering function. In fact, there is a Cantor set of singularities in the scattering function. Chaotic scattering persists over a wide energy range, as shown in Fig. 4(b) for $E=1$.

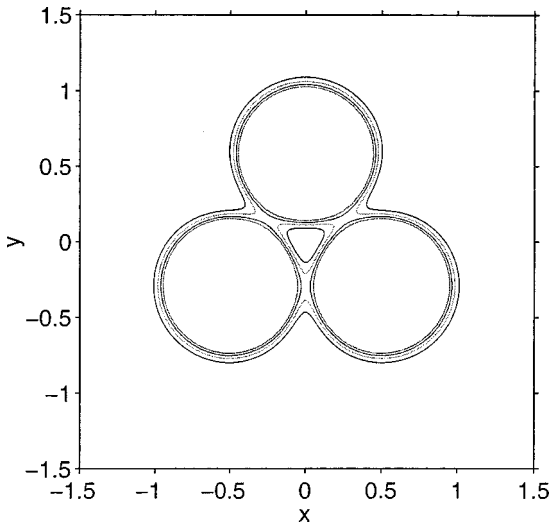

FIG. 3. Contours of three Morse potential hills in the plane $z=0$ for $E=4$, $E=3$, $E=2$, and $E=1$ (inside out, respectively).

The presence of a Cantor set of singularities in the scattering dynamics, as suggested by Figs. 4(a) and 4(b), implies the presence of a chaotic saddle whose fractal dimension in the five-dimensional phase space is larger than 3. This, in general, can be argued as follows. Let D_s and D_u be the

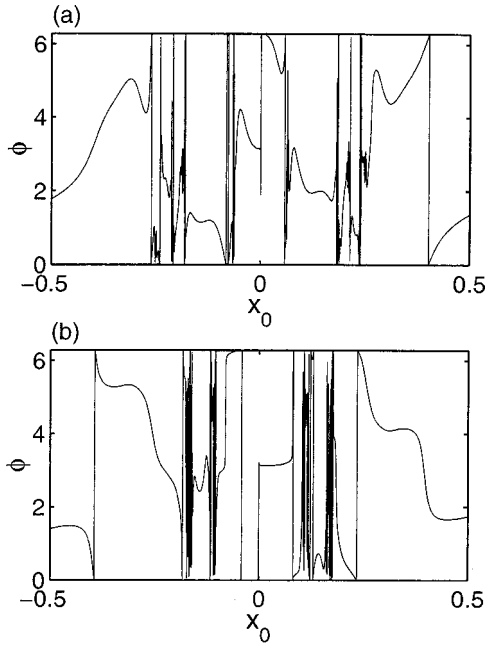

FIG. 4. Scattering function $\phi(x_0)$ for (a) $E=4$ and (b) $E=1$.

dimensions of the stable and unstable foliations of the chaotic saddle in the scattering region. Due to the symplectic nature of Hamiltonian flows, we have $D_s = D_u$. The dimension of the chaotic saddle is given by $D_c = D_s + D_u - N = 2D_s - N$, since, dynamically, the chaotic saddle is the intersecting set between the stable and unstable foliations, where N is the dimension of the phase space. Let $0 < D_0 \leqslant 1$ be the fractal dimension of the Cantor set of singularities probed by a scattering function, which is in fact the set of intersecting points between the stable foliation and the one-dimensional line segment from which particles are launched. We thus have $D_0 = D_s + 1 - N$ or, $D_s = D_0 + N - 1$. This gives for the dimension of the chaotic saddle

$$D_c = 2D_0 + N - 2 = 3 + 2D_0 . \quad (4)$$

Since $0 < D_0 \leqslant 1$ and $N = 5$, we see that $3 < D_c \leqslant 5$. These arguments also suggest that if $D_c < 3$, the scattering function is smooth and, hence, no chaotic behavior can be observed by examining only the scattering function, even though there is a chaotic saddle in the phase space and the scattering dynamics is chaotic [11].

While the scattering functions observed at $E = 4$ [Fig. 4(a)] and at $E = 1$ [Fig. 4(b)] imply the presence of chaotic saddle with $D_c > 3$ in both cases, the dynamical and physical nature of the scattering observed at these energies are expected to be different, because of the topological change in the structure of the invariant set explained in Sec. II. This suggests that there may be a characteristic change in the dynamical invariants of the invariant set in the transition from $E > E_c$ to $E < E_c$.

To verify this, we compute the fractal dimension of the chaotic saddle D_c by using the uncertainty algorithm [16]. Specifically, we randomly choose a large number of pairs of particles at distance ϵ apart from a line segment in the initial plane P_0 and compute, for each pair, whether the two particles exit the scattering region through different planes of the tetrahedron. The fraction of these uncertain pairs $f(\epsilon)$ typically scales with ϵ as $f(\epsilon) \sim \epsilon^{1 - D_0}$, where D_0 is the fractal dimension of the set of singularities in the scattering functions in Figs. 4(a) and 4(b). The dimension of the chaotic saddle is then given by Eq. (4). We find that for $E = 4$, the dimension is $D_c = 4.33 \pm 0.02$, and $D_c = 3.83 \pm 0.02$ for $E = 1$. Figure 5 shows D_c versus E [17] for $1 \leqslant E \leqslant 4$. We see that for $E > E_c$, the dimension remains, roughly, constant. This is due to the structural stability of the chaotic saddle in this energy regime where the potential hills remain isolated and, hence, there is no exponential decrease in the number of unstable periodic orbits. For $E < E_c$, the dimension D_c appears to decrease as E is decreased.

The reason why the fractal dimension decreases as the energy is decreased from E_c can be heuristically understood as follows. Consider initial conditions on a line that contains a Cantor set of singularities. The Cantor set corresponds to particle trajectories that can enter the holes at the side planes of the tetrahedron and stay in the scattering region forever. Those that cannot enter the holes or enter the holes but escape in finite time correspond to gaps between points in the Cantor set. Decreasing the size of the holes is equivalent to enlarging these gaps. For a self-similar Cantor set with primary gap size Δ, its box-counting dimension is given by $D_0 = \ln 2 / \ln[2/(1-\Delta)]$. Assuming that $1 - \Delta$ is proportional to s, the size of the holes, we obtain, using Eq. (3)

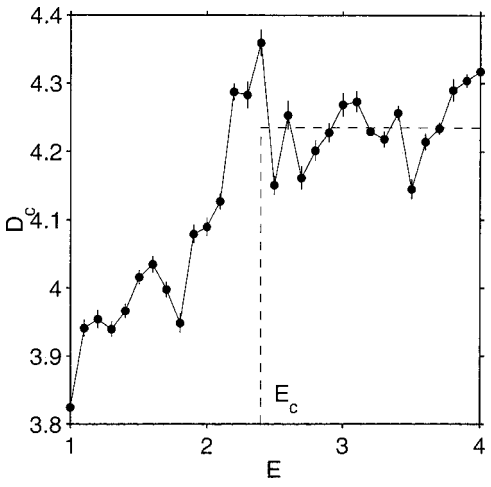

FIG. 5. Fractal dimension D_c of the chaotic saddle versus the energy E. The dimension remains constant for $E > E_c$ and decreases as E is decreased through E_c.

$$D_0 \sim (A - B \ln s)^{-1} \sim \{A - B \ln[c - h(E_c)\Delta E]\}^{-1}, \quad (5)$$

for $E \lesssim E_c$, where A and B are positive constants. This scaling relation indicates that the fractal dimension of the chaotic saddle decreases as the energy E is decreased from the metamorphosis point E_c, due to the shrinkage of the holes on the side planes of the potential configuration. The inverse logarithmic dependence on ΔE of D_0 in the relation is apparently not resolved in our numerical experiments.

We notice that at energies about $E = 1$, chaotic scattering does not occur if the system only has two degrees of freedom, such as the configuration of three potential hills in the plane which has been studied extensively [18,8,9]. This can be understood by plotting the contour of potential hills in the plane, as done in Fig. 3 for $E = 4$ (thick lines) and $E = 1$ (thin lines), respectively. We see that at $E = 4$, the classically forbidden regions are isolated, allowing the formation of chaotic saddles [8,9] in both two- and three-degree-of-freedom Hamiltonian systems. However, at $E = 1$, these forbidden regions are connected. Thus, for two-degree-of-freedom systems, no particle coming from outside the scattering region can enter the bounded triangularlike region formed at the center of the potential hills. The dynamics in the bounded triangularlike region is typically made up of chaotic seas mixed with Kol'mogorov-Arnol'd-Moser (KAM) tori. Although there is bounded chaos in this case, it is not accessible for particles from outside and, hence, there is no chaotic scattering. In the case of three-degree-of-freedom potentials, at the same energy $E = 1$, the corresponding classically allowed bounded region in the center of the potential hills is accessible for scattering particles coming from outside. Chaotic scattering is thus possible, which, for this class of scattering systems, is a uniquely high-dimensional phenomenon.

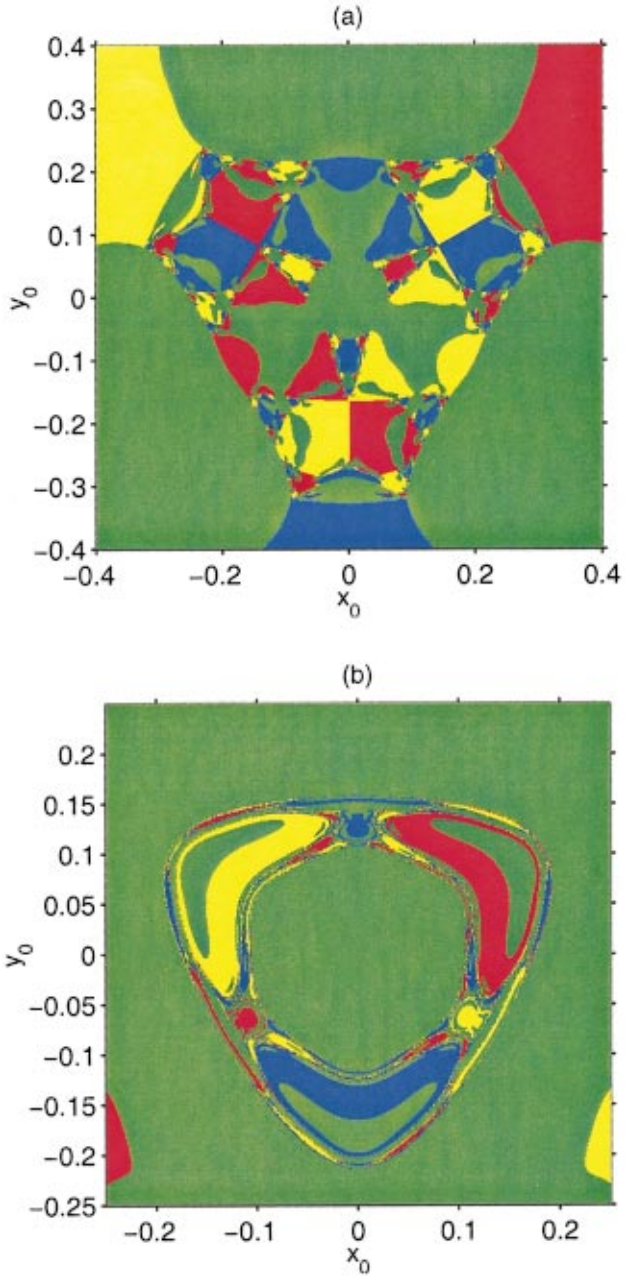

FIG. 6. (Color) Basins of scattering trajectories for (a) $E=4$ and (b) $E=1$. In (a) the basin boundaries common to the four colors consist of completely isolated points. In (b) the part of the basin boundary common to the four colors is connected and it is Wada.

IV. TOPOLOGY OF CHAOTIC SCATTERING

To explore the dynamical consequences of chaotic scattering in different energy regimes, we examine the topology of the scattering dynamics. In particular, we study the basin structure of scattering trajectories. For the tetrahedron configuration, there are four side planes through which particles can exit. Say we launch a large number of particles from a two-dimensional area in an x-y plane at some large negative-z position towards the scattering region. After the scattering, we color code the particles in the initial plane depending on through which plane, formed by any three potentials, they exit the system. Figure 6(a) shows, for $E=4$, the basin structure in the area defined by $(-0.4 \leqslant x_0, y_0 \leqslant 0.4)$ in the plane P_0 located at $z_0=-10.0$. In the computation, 500×500 particles uniformly distributed in the initial area are launched towards the scattering region along the $+z$ direction. If a particle exits through the plane defined by the vertex (1,2,4) shown in Fig. 1 [or (1,3,4), (1,2,3), or (2,3,4)], its location in the initial two-dimensional area is denoted by red (or yellow, blue, or green). As can be seen from Fig. 6(a), the boundary contains isolated points where the four colors meet, but for almost all points in the boundary only two colors meet. Successive enlargement of Fig. 6(a) about any one of these points indicate that these common boundary points are indeed isolated. The basin boundary is the set of intersecting points between the stable manifold of the chaotic saddle with the initial plane P_0. For this energy, then, the set of common boundary points with four colors is isolated. As the energy is lowered, the previously classically forbidden regions become connected and extended parts of the basin boundary points are now common to the four colors, as shown in Fig. 6(b) for $E=1$. This is the Wada property of basins [19,20]. We see that the topology of the basin undergoes a sudden change (metamorphosis) from being disconnected to being Wada at the critical energy value E_c. This metamorphosis is a uniquely higher-dimensional phenomenon which has no counterpart in two degrees of freedom systems—it is a consequence of the topological change of the forbidden region from disconnected to connected as E goes through E_c, as we now explain.

First consider the case $E>E_c$, when the forbidden regions are disconnected [Fig. 2(a)]. A scattering trajectory will typically enter the scattering region, bounce off the forbidden regions a number of times, and leave. As a particle leaves the scattering region, it crosses one of the side planes shown in Fig. 1. For typical trajectories, one can continuously change the initial conditions so as to cause a continuous change in the trajectory (this is not true if the initial condition lies on the stable manifold of the invariant set, but such points have zero measure in phase space). In other words, there are paths in the space of initial conditions such that the escape parameters (such as escape angles, escape time, etc.) change continuously, and these paths contain all initial conditions except for a set of null measure. We now consider a subspace M in the full space of initial conditions; we choose M to have dimension 2 or higher. Consider one such path, denoted C, that connects two points a and b in M belonging to two different escape basins, denoted by S_1 and S_2. Distinct side planes (which define the different escapes) are separated by segments which connect two adjacent triangular faces (Fig. 1). For $E>E_c$, part of these segments lies outside the forbidden regions. Therefore, we can choose the path C in M such that the corresponding trajectories go from one escape to a neighboring one continuously, without going through any other escape; in other words, all points in C belong to either S_1 or S_2. This corresponds to a basin boundary that separates only two escapes, and therefore to a non-Wada basin. The points for which this construction cannot be made are those on the stable manifold of the invariant set, which do not escape after entering the scattering region. All this means that in a surface of initial conditions one can think of the escape basin in many ways as a usual four-colored ''world'' map, each ''country'' being a different escape. As in this case, a boundary point in a usual four-colored map

typically separates only two colors, and points which separate three or more colors are isolated. Of course, the scattering basin ''map'' is different from a usual map in that it is fractal, and has ''country'' structures of arbitrarily small size.

The picture described above completely changes when the energy goes below E_c. The forbidden regions are now connected into one single region, and the boundaries between the side planes that define the different escapes lie entirely within it. It is clear that the construction described above does not work here, since one can no longer go smoothly from one escape to another by a continuous change of initial conditions, due to the presence of forbidden regions separating the escape routes. Consider again a path C in M connecting points a and b belonging to different escape basins S_1 and S_2. As we follow C, the corresponding orbits will eventually come close to the forbidden region that separates the two faces of the tetrahedron corresponding to escapes S_1 and S_2, and will be more and more deflected by it as we pick initial conditions further along C. At some point along the path, the deflection will be large enough to make typical orbits escape by a third side plane, and exit through an escape route that is different from S_1 and S_2. This means that between any two points a and b in C, with $a \in S_1$ and $b \in S_2$, there exists a point c which does not belong to either S_1 and S_2. Since this argument holds for any path C in the space of initial conditions connecting two points belonging to distinct basins, no matter how close they are, the above implies that typical boundary points have the Wada property, as can be seen in Fig. 6(b).

An important point is that the above change in the topological structure of the escape basin is only possible in three-dimensional space, and does not happen for two-degrees-of-freedom systems, where the basin boundary of systems with three or more escapes typically has the Wada property. The reason is that the forbidden regions separating distinct escapes can never be bypassed as one goes from one escape to another, as can be seen from a quick glance at Fig. 3. As explained earlier, when the forbidden regions become connected, the inner region becomes inaccessible to particles coming from outside and there is no chaotic scattering.

V. INVARIANT PLANES AND THE METAMORPHOSIS DYNAMICS

For $E > E_c$, the forbidden region consists of four disconnected pieces, centered on the four vertices of the tetrahedron of Fig. 1. The orbit of a particle inside the scattering region can be understood as doing a series of bounces off the forbidden regions (at least to a first approximation). Because the regions are disconnected, a particle can go from one region to any one of the other three. If we associate the symbols {1, 2, 3, 4} with the forbidden regions, an orbit in the invariant set can be described by a bi-infinite sequence of symbols $\cdots a_{-1} a_0 a_1 a_2 \cdots$, with each a_n belonging to the set {1, 2, 3, 4}, the only rule being that the same symbol cannot occur twice in a row. This symbolic dynamics is equivalent to a full shift on three symbols. All this implies that the dynamics for $E > E_c$ is qualitatively similar to that of four hard balls on a tetrahedron configuration, studied in [11].

This is no longer true, however, for $E < E_c$. For those energies, the periodic orbits that connected pairs of forbidden regions do not exist, since the forbidden region is now one single connected piece, and therefore we expect the symbolic dynamics and the invariant set to be different. In order to better understand the change in the dynamics as E goes below E_c, we look at what happens on the invariant symmetric planes of the potential.

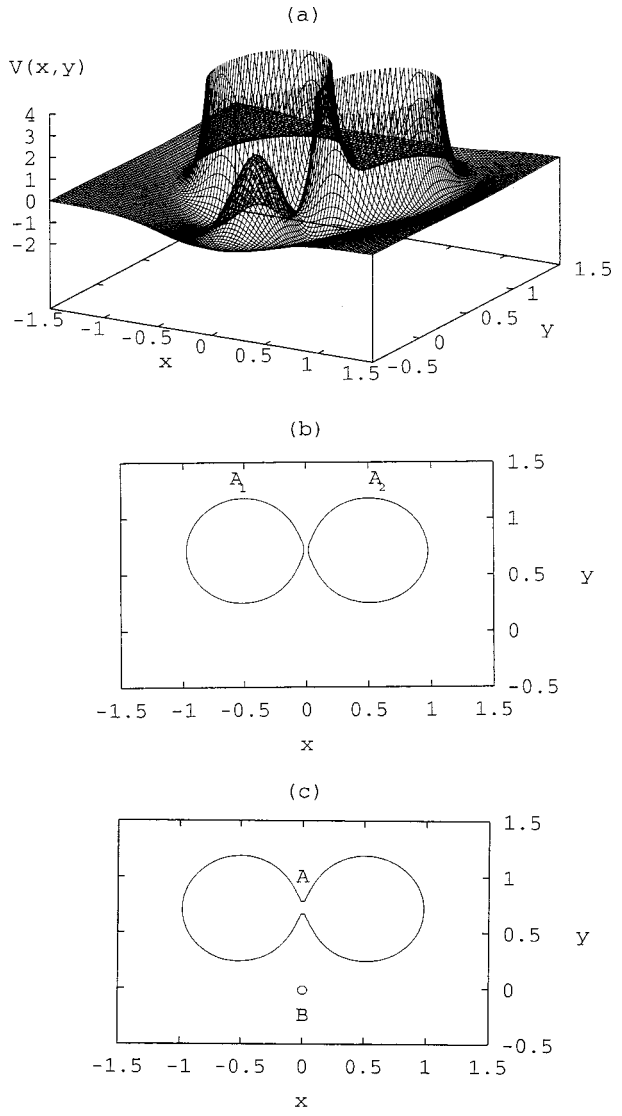

FIG. 7. (a) shows the potential restricted to the invariant plane, (b) shows the equipotential contour $E = 2.14$, and (c) shows the contour $E = 2.5$.

Due to the spatial symmetry of the potential (2), there are six invariant planes, such that if a particle is on one of these planes with a velocity vector in the plane, it never leaves it, because the component of the force perpendicular to the plane vanishes. Spatial reflection about these planes leaves $V(\mathbf{x})$ unchanged. Each such plane cuts through the center of two vertices of the tetrahedron and crosses the midpoint of the segment connecting the other two vertices. In the potential configuration we have chosen the xz plane as a symmetry plane.

Figure 7(a) shows the potential V restricted to one of the symmetry planes; the picture is the same for each of the other five planes. For $E > E_c$, the forbidden region restricted

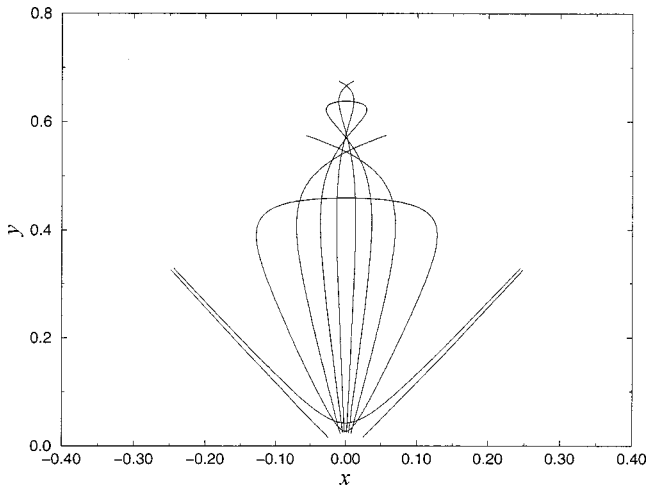

FIG. 8. Periodic orbits for $E=2.14$.

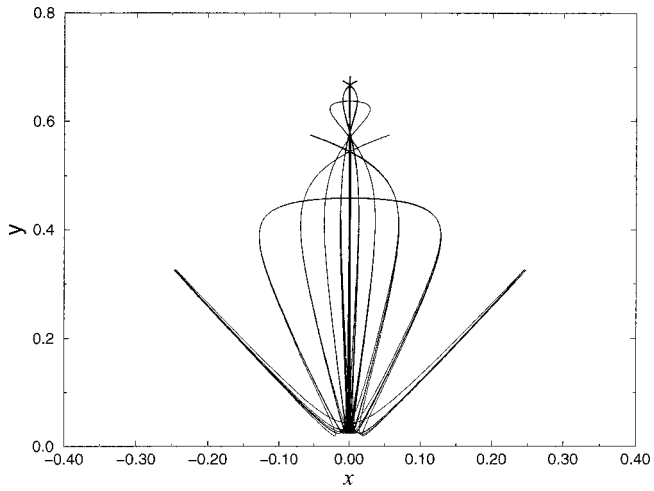

FIG. 9. One single trajectory in the invariant set, followed for a long time, for $E=2.14$.

to the symmetry plane consists of two disconnected regions centered about the vertices lying in the plane, as is seen in Fig. 7(b). We denote the two forbidden regions by A_1 and A_2. For this energy, the only periodic orbit in the plane is the orbit bouncing back and forth between A_1 and A_2; this is true for all energies above E_c. There are six such orbits, each one lying in one of the symmetry planes, each one connecting a pair of forbidden regions.

As E is decreased through E_c, A_1 and A_2 are joined, forming a single connected forbidden region A, and the periodic orbit that connected A_1 and A_2 is destroyed. However, there is a new forbidden region B in the symmetry plane, given by the intersection of the symmetric plane and the forbidden region connecting the two other vertices that are off the plane. This is shown in Fig. 7(c). The appearance of this new forbidden region and the connection of the two previously disconnected regions represent a topological change on the accessible phase space of the system, implying a corresponding topological change (metamorphosis) in the dynamics. The metamorphosis consists of the destruction of the periodic orbits connecting pairs of forbidden regions with the simultaneous creation of new orbits, due to the newly created forbidden regions. Some of the new periodic orbits created in the metamorphosis can be seen in Fig. 8, which shows orbits for $E=2.14$, slightly below the critical energy $E_c \approx 2.25$. The periodic orbits shown in Fig. 8 are the fundamental periodic orbits of the system (for this energy), in the sense that any orbit in the invariant set can be thought of as made of ''pieces'' of these orbits (approximately). This fact is illustrated in Fig. 9, which shows an orbit in the invariant set, calculated by the proper-interior-maximum (PIM) triple method [21]. Comparing Fig. 8 with Fig. 9, we can see that a typical trajectory in the invariant set follows closely one of the periodic orbits shown in Fig. 8, and then, as it approaches the region surrounding B where the fundamental periodic orbits are close to each other, it may follow another periodic orbit, and so on. Each periodic orbit can be associated with a symbol, and thus each orbit in the invariant set is associated with a bi-infinite sequence of symbols.

To each periodic orbit in Fig. 8 we can associate n, the number of successive bounces that a given orbit makes off A without approaching B. For $E>E_c$, there is a periodic orbit that bounces off A_1 and A_2 an infinite number of times approaching B. For $E<E_c$, however, the gap between A_1 and A_2 is closed, and orbits can no longer make consecutive bounces off A an arbitrary number of times, and there is a maximum number of bounces $n_{\max}(E)$ that an orbit can make, which depends on the energy. Large values of $n_{\max}$ imply a higher number of fundamental periodic orbits $N(E)$. As the energy approaches E_c from below, the number of allowed bounces increases, and goes to infinity as $E \to E_c^-$, and therefore the number of fundamental periodic orbits N goes to infinity, too. The creation of each new fundamental orbit implies the inclusion of new symbols in the symbolic dynamics, as discussed in the previous paragraph, and therefore it implies the creation of an uncountable set of new orbits in the invariant set. Each one of these orbits is created in a homoclinic bifurcation, through a saddle center and a cascade of period-doubling bifurcations. The appearance of each fundamental orbit corresponds to one such homoclinic bifurcation. Each such bifurcation occurs in an energy range ΔE, where there are tangencies between the stable and unstable foliations of the invariant set. Therefore, for these energies the invariant set is not hyperbolic, and there are stable islands surrounded by KAM surfaces embedded in the invariant set. For energies in between the homoclinic bifurcations, however, the invariant set is hyperbolic. As $E \to E_c^-$, the bifurcations become closer and closer in energy, and their corresponding energy range ΔE becomes smaller and smaller, and goes to zero in the limit of $E=E_c$. For $E=E_c$, we have an accumulation of homoclinic bifurcations, meaning that for any neighborhood of E_c (that is, for any interval $[E_c-\delta, E_c]$, no matter how small δ is) there is an infinite number of homoclinic bifurcations, resulting from the creation of an infinite number of fundamental periodic orbits. In the limit $E \to E_c^-$, we have an infinite number of fundamental periodic orbits, and an infinite number of symbols in the corresponding symbolic dynamics. This multitude of orbits is destroyed suddenly as E becomes higher than E_c, being replaced by a single periodic orbit bouncing between regions A_1 and A_2. This happens through a topological change in the phase space (and not by the usual saddle-center and period-doubling bifurcation mechanism).

The above discussion is based on the behavior of orbits in

the symmetry planes of potential (2), which is a lower-dimensional subset of the whole dynamical system. Nevertheless, the understanding of this simpler subsystem is essential for the understanding of the scattering dynamics in the full five-dimensional phase space.

VI. CONCLUSION

In summary, we have uncovered a topological bifurcation (metamorphosis) in high-dimensional chaotic scattering systems, and we explain it in terms of the topological change in the accessible phase space as the energy (or another parameter) is varied. We have given a qualitative analysis and numerical evidence for the behavior of the fractal dimension of the underlying chaotic saddle through this metamorphosis. The change in the structure of the invariant set is studied on an invariant plane of the potential. The scattering configuration studied is physically realistic and, hence, the results of this work are expected to be observable. We should point out that, presently, not much is known about high-dimensional chaotic scattering and transient chaos, which is an important area because of its physical relevance.

ACKNOWLEDGMENTS

Y.C.L. was supported by AFOSR under Grant No. F49620-98-1-0400 and by NSF under Grant No. PHY-9722156. C.G. was supported by ONR (Physics) and by a CNPq/NSF-INT Grant. A.P.S.M. was supported by FAPESP.

[1] See, for example, R. Blümel, Chaos **3**, 683 (1993).
[2] See, for example, P. T. Boyd and S. L. W. McMillan, Chaos **3**, 507 (1993).
[3] See, for example, B. Eckhardt and H. Aref, Trans. Soc. R. London A **326**, 655 (1988); E. Ziemniak, C. Jung, and T. Tél, Physica D **76**, 123 (1994); Á. Péntek, T. Tél, and Z. Toroczkai, J. Phys. A **28**, 2191 (1995).
[4] See, for example, D. W. Noid, S. Gray, and S. A. Rice, J. Chem. Phys. **84**, 2649 (1986); Z. Kovács and L. Wiesenfeid, Phys. Rev. E **51**, 5476 (1995).
[5] See, for example, R. A. Jalabert, H. U. Baranger, and A. D. Stone, Phys. Rev. Lett. **65**, 2442 (1990); Y.-C. Lai, R. Blümel, E. Ott, and C. Grebogi, *ibid.* **68**, 3491 (1992); C. M. Marcus, R. M. Westervelt, P. F. Hopkins, and A. C. Gossard, Chaos **3**, 643 (1993).
[6] T. Tél, in *Directions in Chaos*, edited by Bai-lin Hao (World Scientific, Singapore, 1990), Vol. 3; in *STATPHYS 19*, edited by Bai-lin Hao (World Scientific, Singapore, 1996).
[7] Chaos Focus Issue **3** (4) (1993).
[8] S. Bleher, C. Grebogi, and E. Ott, Physica D **46**, 87 (1990); K.-C. Lai, Phys. Rev. E **60**, R6283 (1999).
[9] M. Ding, C. Grebogi, E. Ott, and J. A. Yorke, Phys. Rev. A **42**, 7025 (1990).
[10] Y.-C. Lai and C. Grebogi, Phys. Rev. E **49**, 3761 (1994).
[11] Q. Chen, M. Ding, and E. Ott, Phys. Lett. A **145**, 93 (1990); D. Sweet, E. Ott, and J. A. Yorke, Nature (London) **399**, 315 (1999).
[12] P. M. Morse, Phys. Rev. **34**, 57 (1929); D. ter Haar, *ibid.* **70**, 222 (1946).
[13] See, for example, J. Heagy and J. M. Yuan, Phys. Rev. A **41**, 571 (1990), and references therein.
[14] L. Verlet, Phys. Rev. **159**, 98 (1967).
[15] Previous studies of planar scattering systems showed that chaotic scattering can arise when the particle energy is decreased through V_0, the height of the potential hills [8]. This energy regime, however, is physically unrealistic in situations such as particle scattering by molecules, where the centers of the potential hills are classically impenetrable.
[16] S. W. McDonald, C. Grebogi, E. Ott, and J. A. Yorke, Physica D **17**, 125 (1985).
[17] For a fixed energy, the uncertainty fraction $f(\epsilon)$ is computed by using 40 values of ϵ in the range $(10^{-5},10^{-1})$. For each ϵ, pairs of initial conditions are chosen randomly until the number of uncertain ones reaches 200. The computation was extremely intensive and was done on a 16-node Beowulf supercomputer.
[18] P. Gaspard and S. A. Rice, J. Chem. Phys. **90**, 2225 (1989).
[19] J. Hocking and G. Young, *Topology* (Addison-Wesley, Reading, MA, 1961). For Wada basins in dissipative chaotic systems, see, for example, J. Kennedy and J. A. Yorke, Physica D **51**, 213 (1991).
[20] L. Poon, J. Campos, E. Ott, and C. Grebogi, Int. J. Bifurcation Chaos Appl. Sci. Eng. **6**, 251 (1996); Z. Toroczkai, G. Károlyi, Á. Péntek, T. Tél, C. Grebogi, and J. Yorke, Physica A **239**, 233 (1997); M. A. Sanjuan, J. Kennedy, C. Grebogi, and J. A. Yorke, Chaos **3**, 125 (1997); J. Kennedy, M. A. Sanjuan, J. A. Yorke, and C. Grebogi, Top. Appl. Phys. **94**, 207 (1999).
[21] H. E. Nusse and J. A. Yorke, Physica D **36**, 137 (1989).